COMBINING PHASE VELOCITY METHOD AND FEM FOR COMPUTING DISPERSION CURVES IN CURVED PLATE GUIDEWAVES.

M. Cruz Rodriguez[†], V. Hernández Mederos, J. Estrada Sarlabous, E. Moreno Hernández, A. Mansur Graverán.
Instituto de Cibernética, Matemática y Física, ICIMAF, La Habana, Cuba

ABSTRACT
Lamb waves are extensively used in non-destructive tests (NDT) to detect corrosion and another defects in thin plates. Several NDT methods require to compute the phase velocity of the Lamb wave, which depends on the frequency. In this work we show the potential of the combination of the *phase velocity method* (PVM) with the *finite element method* (FEM) for computing the phase velocity dispersion curve of an ultrasonic pulse traveling in a transversally annular isotropic thin plate. The *FEM-PVM* is based on the numerical solution of the wave propagation equations for several selected frequencies. To solve these equations, a second order difference scheme is used to discretize the temporal variable, while spatial variables are discretized with FEM. The open software FreeFem++ is used with quadratic triangular elements to compute the displacements. The phase velocity for a given frequency is obtained from the computed displacements at few points on the top of the plate. Repeating the procedure for several frequencies we compute a sample of points that are fitted to obtain an approximation of the phase velocity dispersion curve. A deeper understanding on the behavior of the phase velocity dispersion curve with respect to the plate curvature is obtained as result of an extensive experimentation with annular isotropic plates of two materials.

KEYWORDS: finite element method, phase velocity method, dispersion curve, FreeFem++, curved plate guidewaves waves.

MSC: 65N30, 74S05, 74B05

RESUMEN
Las ondas de Lamb son muy utilizadas en los ensayos no destructivos (NDT) para detectar corrosión y otros defectos en placas delgadas. Varios métodos de NDT requieren calcular la velocidad de fase de la onda de Lamb, la cual depende de la frecuencia. En este trabajo se muestra el potencial de la combinación del *método de la velocidad de fase* (PVM) con el *método de elementos finitos* (FEM), para calcular la curva de dispersión de la velocidad de fase de una onda ultrasónica que viaja a lo largo de una placa transversalmente anular e isótropa. *FEM-PVM* se basa en la solución numérica de las ecuaciones de la propagación de ondas para varias frecuencias seleccionadas. Para resolver estas ecuaciones se usa un esquema en diferencias de segundo orden para discretizar la variable temporal, mientras que las variables espaciales se discretizan con FEM. Para calcular los desplazamientos se utiliza el código libre FreeFem++ con elementos triangulares cuadráticos. La velocidad de fase para una frecuencia dada se obtiene a partir de los desplazamientos calculados en unos pocos puntos situados en la superficie superior de la placa. Repitiendo este procedimiento para varias frecuencias se calcula una muestra de puntos, los cuales se ajustan para obtener una aproximación de la curva de dispersión de la velocidad de fase. El trabajo permite obtener una comprensión más profunda del comportamiento de la curva de dispersión de la velocidad de fase con respecto a la curvatura de la placa a partir de una extensa experimentación numérica con placas isotrópicas anulares de dos materiales.

PALABRAS CLAVE: Método de elementos finitos, método de velocidad de fase, curva de dispersión, FreeFem++, guias de onda curvas.

[†]manuel@icimaf.cu

1. INTRODUCTION

In today's industry, plate-like structures are present in many areas such as energy and petrochemical industries, in building structures, pipelines of gases and liquids and in the study of aeronautical and aerospace structures [11, 18, 19]. In these fields of industry the good structural state of its components is very important since a premature failure can be very expensive or disastrous. In order to avoid these failures, often non-destructive testing (NDT) are used in component inspections [3].
Lamb waves have the property to propagate long distances along thin structures [15], because they use the structure itself as a waveguide. Hence, they are suitable to inspect hidden or difficult to access areas, such as partially buried structures covered with protective or insulating material or structures hidden behind other elements.
In order to carry out these inspections properly, it is necessary to know a priori the elasto-dynamic behavior of the inspected structure. How Lamb waves propagate along the structures to be evaluated and how they interact with possible defects may be characterized by means of their phase velocity. Lamb waves are dispersive, i.e., their propagation velocities and mode shapes are frequency dependent. This phenomenon is known as geometric dispersion and it is represented by the geometric *dispersion curves* [12], which describe the non trivial relationship between phase velocity and frequency. The dispersion curve is indispensable in the calibration of ultrasonic equipments to study the position and size of defects, with a procedure based on a pitch-catch configuration. The idea of this procedure is that in presence of flaws, such as corrosion or delaminations, breaks in the material homogeneity produce, for a given frequency, a value of the measured phase velocity that does not agree with the value predicted by the dispersion curve. In this sense, dispersion curves are very important for NDT applications dealing with thin isotropic curved plates, such as tank containers and curved metallic structures.
Dispersion curves can be obtained analytically when the material has a simple geometry. This is for example the case of bars and flat plates, however in the case of more general geometries there are no analytical models and numerical simulation is needed.

1.1. Related works

Due its importance in applications, several methods to compute dispersion curves may be found in the literature. A nice recent comparative study of mathematical methods for calculating dispersion curves in plates is presented in [21]. In that paper the most common methods for wave propagation analysis are compared, such as the exact $3D$ elasticity theory based methods (global matrix, stiffness matrix, hybrid compliance-stiffness matrix) as well as the approximate methods (semi analytical finite element, Legendre polynomial, fifth order shear deformation theory).
The numerical simulation of guided Lamb wave propagation in particle-reinforced flat composites is considered in [24]. The finite element method is used to perform parameter studies in order to better understand how the propagation of the Lamb waves in these flat plates is affected by changes in the central frequency of the excitation signal. The Spectral finite element Method, the hierarchical p-FEM and the IgA approach are compared in [25], where they are used to compute the time-of-flight of Lamb waves propagating along a flat plate of finite length. Phase velocity method was introduced initially as an experimental method to evaluate flat specimens of constant thickness. In [16, 17] it was used with continuous excitation. Later, it was extended and validated for pulses in [16, 17, 19, 20]. It was also applied to evaluate experimentally laminations in aircrafts using ultrasonic pulses, due to the strong dependence of the velocity on thickness [20].
For flat plates of constant thickness, at a given frequency, each propagating Lamb wave has a constant phase velocity and a constant wavenumber. On the other hand, in modern industry it is frequently required to test planar waveguides with continuous variation of thickness. The propagation of adiabatic modes in an elastic planar plate with a slowly linearly varying thickness is considered in [7, 9, 22]. When the waves propagate in direction to decreasing thickness it becomes apparent, in both the experiments and the simulations, that a critical thickness could be reached corresponding to their cut-off. Reflection and conversion phenomena have then been observed.

The phase velocity and the mode shapes have been examined at various curvatures using a 2D *circumferential* waveguide problem to study the curvature effect in [10]. The paper presents an experimental study to validate the analytical predictions. The experiment involved a sensitive measurement of the change of velocity as the curvature of a waveguide was increased.

1.2. Our contribution

The main contribution of this work is to show the potential of the use of the combination *FEM-PVM* for the numerical computation of the phase velocity dispersion curve of an ultrasonic pulse traveling in a thin curved plate guidewave. Our work is focused on the case of thin isotropic curved plate guidewaves with constant thickness and it could be extended to guided modes of waveguides propagating in thin orthotropic and homogeneous curved plates, composed of several layers of carbon fabrics in resin. A FreeFem++ in-house code for computing approximately the pulse displacement and the plate deformation field has been implemented and it is available at GitHub [5]. The numerical experiments with *FEM-PVM* shown in this work provide new information on Lamb waves propagating along thin curved plates, in particular on the behavior of the phase velocity dispersion curves with respect to small variations of the curvature or the thickness.

2. THE WAVE PROPAGATION PROBLEM ON A PLATE

2.1. Formulation of the problem

In the wave propagation problem solved here it is assumed symmetry with respect to the z-axis and zero displacement in the z-direction. Therefore, the wave propagation problem is represented as a two-dimensional *plane strain* model in the $x-y$ plane [23, 1]. Physical damping is not included. The physical domain Ω of the problem is a finite 2D annular sector, as shown in the Figure 1, with boundary $\partial\Omega$ equal to the union of δ_1 and δ_2. Given a curvature value $\kappa > 0$ and $L_y > 0$ the (constant) thickness of Ω, the radius of the middle circle arc of Ω, is $R_m = \frac{1}{\kappa}$, the radius of the outer circle arc is $R_2 = R_m + \frac{L_y}{2}$ and the radius of the inner circle arc is $R_1 = R_m - \frac{L_y}{2}$. The annular sector angle is θ (in radians) and the arc length of middle circle arc of Ω is $L_x = \frac{\theta}{\kappa}$.

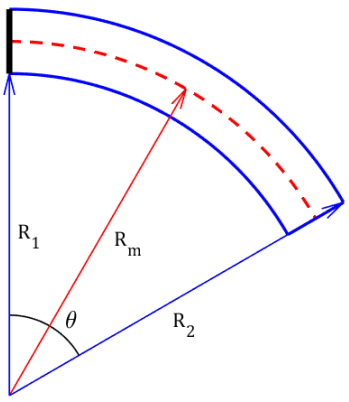

Figure 1: Geometry of the physical domain Ω. Boundaries δ_1 (blue) and δ_2 (black).

The pulse used to generate pure antisymmetric Lamb modes such as A_0 is a signal in the y-direction at the left boundary δ_2 of the plate. It is described by the function,

$$g(t) = \phi \, \sin\left(2\,\pi\, f_0\, t\right) \mathrm{e}^{-\beta\, {f_0}^2 \left(t - \frac{9}{4 f_0}\right)^2} \quad \text{for} \quad t \geq 0 \tag{2.1}$$

where $\phi = 10^{-3}\, m$ is the pulse amplitude and $\beta = 0.9134221$. The parameter f_0 defining $g(t)$ is the frequency. In the experiments of section 5. we consider 10 different values for f_0. Figure 2 shows the graph of a typical pulse $g(t)$ obtained for $f_0 = 0.5\ MHz$.

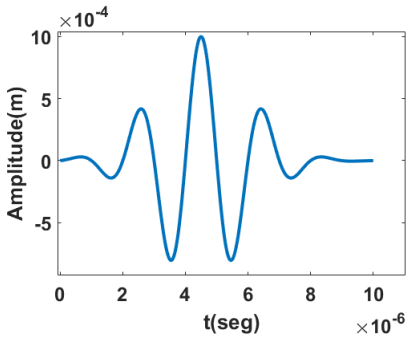

Figure 2: Pulse $g(t)$ in (2.1) applied to the left boundary δ_2 of the plate for $f_0 = 0.5\ MHz$ and $\phi = 1.0 \cdot 10^{-3}\ m$.

The propagation of the pulse in the plate is modeled as a wave propagation problem. Hence, the displacement is a vectorial function $\boldsymbol{u}(t, x, y) = (u_x(t, x, y), u_y(t, x, y))$, depending on the temporal variable t, the spatial variables $\boldsymbol{x} = (x, y)$, the density of the material ρ and the elasticity coefficients. Transversally isotropic materials, depend on 4 elasticity coefficients, that in Voigt nomenclature are denoted as C_{11}, C_{66}, C_{22} and C_{12}. Recall that in the isotropic case $C_{12} = \lambda$, $C_{66} = \mu$ and $C_{11} = C_{22} = \lambda + 2\mu$, where λ and μ are the Lamé constants.
In linear elasticity theory the strain tensor $\boldsymbol{S}(\boldsymbol{u})$ is defined as,

$$\boldsymbol{S}(\boldsymbol{u}) = \begin{pmatrix} S_{11}(\boldsymbol{u}) & S_{12}(\boldsymbol{u}) \\ S_{21}(\boldsymbol{u}) & S_{22}(\boldsymbol{u}) \end{pmatrix} = \begin{pmatrix} \dfrac{\partial u_x}{\partial x} & \dfrac{1}{2}\left(\dfrac{\partial u_x}{\partial y} + \dfrac{\partial u_y}{\partial x}\right) \\ \dfrac{1}{2}\left(\dfrac{\partial u_x}{\partial y} + \dfrac{\partial u_y}{\partial x}\right) & \dfrac{\partial u_y}{\partial y} \end{pmatrix} \tag{2.2}$$

Moreover, according to Hooke's law [23], the stress tensor $\boldsymbol{\sigma}(\boldsymbol{u})$ can be written in terms of the strain as,

$$\boldsymbol{\sigma}(\boldsymbol{u}) = \begin{pmatrix} C_{12}S_{22}(\boldsymbol{u}) + C_{11}S_{11}(\boldsymbol{u}) & 2C_{66}S_{12}(\boldsymbol{u}) \\ 2C_{66}S_{12}(\boldsymbol{u}) & C_{12}S_{11}(\boldsymbol{u}) + C_{22}S_{22}(\boldsymbol{u}) \end{pmatrix} \tag{2.3}$$

With this expression for $\boldsymbol{\sigma}(\boldsymbol{u})$, the function $\boldsymbol{u}(t, x, y)$ is solution of the system of partial differential equations of motion [23],

$$\rho \frac{\partial^2 \boldsymbol{u}}{\partial t^2} = \nabla \cdot \boldsymbol{\sigma}(\boldsymbol{u}) \tag{2.4}$$

In δ_2 the Dirichlet boundary condition,

$$\boldsymbol{u}(t, \boldsymbol{x}) = (0, g(t)), \quad \boldsymbol{x} \in \delta_2 \tag{2.5}$$

is imposed. Moreover, we assume that boundaries δ_1 are free, which means that Neumann boundary conditions

$$\boldsymbol{\sigma}(\boldsymbol{u}(t, \boldsymbol{x})) \cdot \boldsymbol{n}(\boldsymbol{x}) = \boldsymbol{0}, \quad \boldsymbol{x} \in \delta_1 \tag{2.6}$$

hold, where $\boldsymbol{0} = (0, 0)$ and $\boldsymbol{n}(\boldsymbol{x})$ is the vector normal to the boundary of the plate in the point $\boldsymbol{x}$. Finally, the problem is solved in the temporal interval $t \in [0, t_f]$, with $t_f > 0$ given. The initial conditions

$$\begin{aligned} \boldsymbol{u}(0, \boldsymbol{x}) &= \boldsymbol{0}, \quad \boldsymbol{x} \in \Omega \\ \frac{\partial \boldsymbol{u}}{\partial t}(0, \boldsymbol{x}) &= \boldsymbol{0}, \quad \boldsymbol{x} \in \Omega \end{aligned} \tag{2.7}$$

are also imposed.

3. NUMERICAL SOLUTION OF THE WAVE PROPAGATION PROBLEM

3.1. Finite difference discretization of time

In the literature, the most common approach to solve numerically transient problems consists in using a FEM discretization of the spatial variables, keeping continuous the temporal variable. That leads to a system of linear ordinary differential equations, which may be integrated by means of different methods, see for instance [2, 25]. In the present work, we discretize first the second derivative of the displacement with respect to time t, building a uniform mesh $t_i = i \cdot \Delta t$ in the interval $[0, t_f]$, with step Δt, and using a *backward difference* formula, with $O(\Delta t^2)$ approximation error,

$$2\rho \boldsymbol{u}(t_i, \boldsymbol{x}) - (\Delta t)^2 \nabla \cdot \sigma(\boldsymbol{u}(t_i, \boldsymbol{x})) = \rho \left(5\boldsymbol{u}(t_{i-1}, \boldsymbol{x}) - 4\boldsymbol{u}(t_{i-2}, \boldsymbol{x}) + \boldsymbol{u}(t_{i-3}, \boldsymbol{x})\right), \quad \boldsymbol{x} \in \Omega, i = 1, ..., N \tag{3.1}$$

Thus, introducing the notation $\boldsymbol{u}_i(\boldsymbol{x}) = \boldsymbol{u}(t_i, \boldsymbol{x})$, our problem is reduced to find for each fixed time $t = t_i$, $i = 1, ..., N$, a function $\boldsymbol{u}_i(\boldsymbol{x})$ that satisfies the partial differential equations (3.1) with boundary conditions,

$$\boldsymbol{u}_i(\boldsymbol{x}) = (0, g(t_i)), \quad \boldsymbol{x} \in \delta_2 \tag{3.2}$$

$$\boldsymbol{\sigma}(\boldsymbol{u}_i(\boldsymbol{x})) \cdot \boldsymbol{n}(\boldsymbol{x}) = \boldsymbol{0}, \quad \boldsymbol{x} \in \delta_1 \tag{3.3}$$

Functions $\boldsymbol{u}_i(\boldsymbol{x})$ for $i = 2, ..., N$ are computed using (3.1). From the initial conditions (2.7), we set

$$\boldsymbol{u}_0(\boldsymbol{x}) = \boldsymbol{0}, \quad \boldsymbol{u}_{-1}(\boldsymbol{x}) = \boldsymbol{0}, \quad \boldsymbol{x} \in \Omega \tag{3.4}$$

Central difference method [2] is used to compute $\boldsymbol{u}_1(\boldsymbol{x})$ from $\boldsymbol{u}_{-1}(\boldsymbol{x})$ and $\boldsymbol{u}_0(\boldsymbol{x})$.

3.2. Finite element discretization of spatial variables

In this section we use FEM to solve, for each fixed time $t = t_i$, partial differential equations (3.1) depending on spatial variables $\boldsymbol{x}$. Since the time is frozen, the variational formulation of the problem is mathematically studied in functional spaces where the norm does not include the time dependency.

3.2.1. Variational formulation

Let us consider the variational formulation of the problem (3.1) with homogeneous Dirichlet boundary condition,

$$\boldsymbol{u}_i(\boldsymbol{x}) = (0, 0), \quad \boldsymbol{x} \in \delta_2 \tag{3.5}$$

Recall that if $\boldsymbol{u}_i(\boldsymbol{x})$ is the solution of problem (3.1), with boundary conditions (3.3) and (3.5), then the solution of the original problem with nonhomogeneous Dirichlet condition (3.2), is obtained adding to $\boldsymbol{u}_i(\boldsymbol{x})$ a function $\boldsymbol{ug}_i(\boldsymbol{x})$ with,

$$\boldsymbol{ug}_i(\boldsymbol{x}) = \begin{cases} \boldsymbol{0}, & \boldsymbol{x} \in \Omega \setminus \delta_2 \\ (0, g(t_i)), & \boldsymbol{x} \in \delta_2 \end{cases} \tag{3.6}$$

To obtain the variational formulation of the problem (3.1) with homogeneous Dirichlet condition we consider the Hilbert space $\mathcal{V}_0$ of functions

$$\mathcal{V}_0 = \{\boldsymbol{v} \in H^2(\Omega) \times H^2(\Omega) : \ \boldsymbol{v}|_{\delta_2} = \boldsymbol{0}\} \tag{3.7}$$

Since functions in $\mathcal{V}_0$ vanish on a section of the boundary of Ω, the scalar product $\langle \boldsymbol{u}, \boldsymbol{v} \rangle_{\mathcal{V}_0}$ of functions $\boldsymbol{u} = (u_x, u_y)$ and $\boldsymbol{v} = (v_x, v_y)$ in $\mathcal{V}_0$ can be defined as,

$$\langle \boldsymbol{u}, \boldsymbol{v} \rangle_{\mathcal{V}_0} = \iint_{\Omega} (\nabla u_x \cdot \nabla v_x + \nabla u_y \cdot \nabla v_y) d\boldsymbol{x} \tag{3.8}$$

The variational formulation of the problem is obtained, as usual, computing the scalar product of both members of equation (3.1) with a function $\boldsymbol{v} \in \mathcal{V}_0$ and integrating the product over Ω,

$$2\rho \iint_{\Omega} \boldsymbol{u}_i(\boldsymbol{x}) \cdot \boldsymbol{v}(\boldsymbol{x})\, d\boldsymbol{x} - \Delta t^2 \iint_{\Omega} \nabla \cdot \boldsymbol{\sigma}(\boldsymbol{u}_i(\boldsymbol{x})) \cdot \boldsymbol{v}(\boldsymbol{x})\, d\boldsymbol{x} = \rho \iint_{\Omega} \boldsymbol{f}_i(\boldsymbol{x}) \cdot \boldsymbol{v}(\boldsymbol{x})\, d\boldsymbol{x} \tag{3.9}$$

where

$$\boldsymbol{f}_i(\boldsymbol{x}) := 5\boldsymbol{u}_{i-1}(\boldsymbol{x}) - 4\boldsymbol{u}_{i-2}(\boldsymbol{x}) + \boldsymbol{u}_{i-3}(\boldsymbol{x}) \tag{3.10}$$

The second summand in the left hand side of (3.9) can be significantly simplified using Green's identity and taking into account boundary conditions (3.3) and (3.5). The resulting integral can be written in terms of the strain tensor as,

$$-\iint_{\Omega} (\nabla \cdot \boldsymbol{\sigma}(\boldsymbol{u}(\boldsymbol{x}))) \cdot \boldsymbol{v}(\boldsymbol{x})\, d\boldsymbol{x} = 2\mu \iint_{\Omega} \boldsymbol{S}(\boldsymbol{u}(\boldsymbol{x})) : \boldsymbol{S}(\boldsymbol{v}(\boldsymbol{x}))\, d\boldsymbol{x} + \lambda \iint_{\Omega} (\nabla \cdot \boldsymbol{u}(\boldsymbol{x}))(\nabla \cdot \boldsymbol{v}(\boldsymbol{x}))\, d\boldsymbol{x} \tag{3.11}$$

where the **:** contraction operator is defined in [14], Ch. 11. Substituting (3.11) in (3.9) we obtain the variational formulation of problem (3.1) with boundary conditions (3.3) and (3.5):

Find $\boldsymbol{u}_i \in \mathcal{V}_0$ such that for all $\boldsymbol{v} \in \mathcal{V}_0$,

$$a(\boldsymbol{u}_i, \boldsymbol{v}) = F(\boldsymbol{v}) \tag{3.12}$$

where

$$\begin{aligned} a(\boldsymbol{u}, \boldsymbol{v}) &= 2\rho \iint_{\Omega} \boldsymbol{u}(\boldsymbol{x}) \cdot \boldsymbol{v}(\boldsymbol{x})\, d\boldsymbol{x} + 2\mu(\Delta t)^2 \iint_{\Omega} \boldsymbol{S}(\boldsymbol{u}(\boldsymbol{x})) : \boldsymbol{S}(\boldsymbol{v}(\boldsymbol{x}))\, d\boldsymbol{x} \\ &+ \lambda(\Delta t)^2 \iint_{\Omega} (\nabla \cdot \boldsymbol{u}(\boldsymbol{x}))(\nabla \cdot \boldsymbol{v}(\boldsymbol{x}))\, d\boldsymbol{x} \qquad (3.13) \\ F(\boldsymbol{v}) &= \rho \iint_{\Omega} \boldsymbol{f}_i(\boldsymbol{x}) \cdot \boldsymbol{v}(\boldsymbol{x})\, d\boldsymbol{x} \qquad (3.14) \end{aligned}$$

with $\boldsymbol{f}_i(\boldsymbol{x})$ given by (3.10).

The existence and uniqueness of the solution $\boldsymbol{u}_i \in \mathcal{V}_0$ of the variational problem (3.12)-(3.14) for thin curved plates, as well as an *a priori* error estimate in the L^2 norm, may be proven following similar arguments as those used in [6] for thin flat plates. Therefore, their proofs for thin curved plates are not included.

3.2.2. The Galerkin approach

The Galerkin method solves the variational problem (3.12)-(3.14) looking for an approximated solution in a finite-dimensional subspace $\mathcal{V}_0^h$. In the classical FEM, this subspace is defined in terms of a partition of the physical domain Ω in a mesh of triangles or quadrilaterals. In this paper, we discretize Ω constructing a mesh of N_t triangles Δ_r of size h_r, with $r = 1, ..., N_t$ such that $\cup_{r=1}^{N_t} \Delta_r = \Omega$. The triangular mesh is denoted by τ^h, where $h = \max\limits_{1 \le r \le N_t} h_r$ represents the *size of the triangulation*. We choose to use a conforming finite element method, i.e., $\mathcal{V}_0^h$ is a subspace of the space $\mathcal{V}_0$, and the bilinear form and the linear form of the discrete problem are identical to the original ones, see [4]. Denote by $\boldsymbol{x}_j$ for $j = 1, ..., N_m$ the nodes of the mesh τ^h. Assume that the nodes $\boldsymbol{x}_j$ have been numbered in such a way that for $j = 1, ..., N_n$, $\boldsymbol{x}_j \notin \delta_2$, with $N_n < N_m$. Denote by $\mathbb{P}^k(\tau^h)$ the space of functions that restricted to each triangle Δ_r are polynomials of degree $\le k$. Then our space $\mathcal{V}_0^h$ is defined as,

$$\mathcal{V}_0^h = \left\{ \boldsymbol{u}^h \in \mathbb{P}^k(\tau^h) \times \mathbb{P}^k(\tau^h) : \boldsymbol{u}^h \in C^0(\Omega) \times C^0(\Omega) \ \textit{and} \ \boldsymbol{u}^h(\boldsymbol{x}_j) = 0, \ \ j = N_n + 1, ..., N_m \right\} \tag{3.15}$$

Denote by $\phi_r(\boldsymbol{x}),\ \ r=1,...,N_n$ the classical *Lagrange functions* (corresponding to the nodes $\boldsymbol{x}_j \notin \delta_2$) which satisfy

$$\phi_r(\boldsymbol{x}_j) = \begin{cases} 1, & r=j \\ 0, & r \neq j \end{cases}, \ \ j,r=1,...N_n \tag{3.16}$$

For a fixed time $t=t_i$, denote by $\boldsymbol{u}_i^h(\boldsymbol{x})$ the function in $\mathcal{V}_0^h$ approximating $\boldsymbol{u}_i(\boldsymbol{x})$. Since $\boldsymbol{u}_i^h(\boldsymbol{x}) \in \mathcal{V}_0^h$ it can be written as,

$$\boldsymbol{u}_i^h(\boldsymbol{x}) = \left(\sum_{r=1}^{N_n} q_{r,1}^i \phi_r(\boldsymbol{x}), \sum_{r=1}^{N_n} q_{r,2}^i \phi_r(\boldsymbol{x}) \right) = \sum_{r=1}^{N_n} q_{r,1}^i (\phi_r(\boldsymbol{x}),0) + \sum_{r=1}^{N_n} q_{r,2}^i (0,\phi_r(\boldsymbol{x})) \tag{3.17}$$

for certain unknown coefficients $q_{r,1}^i$ and $q_{r,2}^i$ with $r=1,...,N_n$. Observe that according to (3.16), $\left(q_{j,1}^i, q_{j,2}^i\right) = \boldsymbol{u}_i^h(\boldsymbol{x}_j)$, $j=1,...,N_n$. Moreover, vector valued functions $(\phi_r,0),(0,\phi_r)$, $r=1,...,N_n$ define a basis of $\mathcal{V}_0^h$. To simplify the expressions, we use the following notation for basis functions and coefficients,

$$\left(\boldsymbol{\psi}_1, \boldsymbol{\psi}_2, ..., \boldsymbol{\psi}_{2N_n}\right) = ((\phi_1,0),(0,\phi_1),...,(\phi_{N_n},0),(0,\phi_{N_n})) \tag{3.18}$$

$$\left(d_1^i, d_2^i, ..., d_{2N_n}^i\right) = \left(q_{1,1}^i, q_{1,2}^i, ..., q_{N_n,1}^i, q_{N_n,2}^i\right) \tag{3.19}$$

With this notation, (3.17) can be written as

$$\boldsymbol{u}_i^h(\boldsymbol{x}) = \sum_{r=1}^{2N_n} d_r^i \boldsymbol{\psi}_r(\boldsymbol{x}) \tag{3.20}$$

The Galerkin approximation $\boldsymbol{u}_i^h$ to $\boldsymbol{u}_i$ is constructed demanding that it satisfies the variational formulation (3.12)-(3.14)

$$a(\boldsymbol{u}_i^h, \boldsymbol{v}) = F(\boldsymbol{v}) \quad for\ \ all\ \ \boldsymbol{v} \in \mathcal{V}_0^h$$

This is equivalent to require that,

$$a(\boldsymbol{u}_i^h, \boldsymbol{\psi}_j) = F(\boldsymbol{\psi}_j), \quad j=1,...,2N_n \tag{3.21}$$

because functions $\boldsymbol{\psi}_j,\ j=1,...,2N_n$ are a basis of $\mathcal{V}_0^h$. Denote by $\boldsymbol{d}^i = (d_1^i, d_2^i, ..., d_{2N_n}^i)^t$ the vector of coefficients of $\boldsymbol{u}_i^h(\boldsymbol{x})$ in (3.20). Substituting (3.20) in (3.21) and taking into account the linearity of the integral and the strain $\boldsymbol{S}(\cdot)$ operators, we obtain a linear system of equations that can be written in matrix form as,

$$\boldsymbol{A}\,\boldsymbol{d}^i = \boldsymbol{b}^i \tag{3.22}$$

where

$$\boldsymbol{A} = 2\boldsymbol{M} + (\Delta t)^2 \boldsymbol{K} \tag{3.23}$$

with the mass matrix $\boldsymbol{M}$ and the stiffness matrix $\boldsymbol{K}$ given by,

$$\boldsymbol{M} = (M_{rj}) = \rho \iint_\Omega \left(\boldsymbol{\psi}_r \cdot \boldsymbol{\psi}_j\right) d\boldsymbol{x}$$

$$\boldsymbol{K} = (K_{rj}) = 2\mu \iint_\Omega \left(\boldsymbol{S}(\boldsymbol{\psi}_r) : \boldsymbol{S}(\boldsymbol{\psi}_j)\right) d\boldsymbol{x} + \lambda \iint_\Omega (\nabla \cdot \boldsymbol{\psi}_r)(\nabla \cdot \boldsymbol{\psi}_j) d\boldsymbol{x}$$

and $\boldsymbol{b}^i = (b_1^i, ..., b_{2N_n}^i)^t$ with

$$b_j^i = \rho \iint_\Omega \left(\boldsymbol{f}_i \cdot \boldsymbol{\psi}_j\right) d\boldsymbol{x} \tag{3.24}$$

Remarks

1. To compute the approximated solution $\boldsymbol{u}_i^h(\boldsymbol{x})$, for each fixed time $t = t_i$, we have to solve the linear system (3.22). The matrix $\boldsymbol{A}$ depends on the triangular mesh τ^h and on the time step Δt. In particular, for fixed τ^h, if Δt is constant, all systems have the *same matrix* $\boldsymbol{A}$. Matrix $\boldsymbol{A}$ given by (3.23) is sparse, symmetric and positive definite (see [6], Lemma 2.), therefore if Δt is constant it is convenient to compute only once the Cholesky factorization of $\boldsymbol{A}$ to solve the systems by forward and backward substitution.

2. From (3.10) and (3.20) it holds that,

$$\boldsymbol{f}_i = \sum_{r=1}^{2N_n} (5d_r^{i-1} - 4d_r^{i-2} + d_r^{i-3})\boldsymbol{\psi}_r(\boldsymbol{x})$$

   Hence, $\boldsymbol{b}^i$ can be written in terms of the mass matrix $\boldsymbol{M}$ as,

$$\boldsymbol{b}^i = \boldsymbol{M}(5\boldsymbol{d}^{i-1} - 4\boldsymbol{d}^{i-2} + \boldsymbol{d}^{i-3}) \tag{3.25}$$

   From the expressions (3.23) and (3.25), it is clear that the linear system (3.22) resulting from the Galerkin formulation of our problem coincides with the linear system of Houbolt integration scheme [2].

3. The linear system (3.22) has a unique solution. Hence, the Galerkin approximation $\boldsymbol{u}_i^h$, to the solution of the problem (3.1), with boundary conditions (3.3) and (3.5) *exists and it is unique.*

4. To obtain the solution of the problem (3.1)-(3.3) with *non homogeneous Dirichlet* boundary condition (3.2), an approximation $\boldsymbol{ug}_i^h(\boldsymbol{x})$ of the function $\boldsymbol{ug}_i(\boldsymbol{x})$ given in (3.6) must be computed. According to the previous ordering, the nodes $\boldsymbol{x}_j$ for $j = N_n + 1, ..., N$ are in δ_2. The approximation $\boldsymbol{ug}_i^h(\boldsymbol{x})$ is computed requiring that it interpolates the function $\boldsymbol{ug}_i(\boldsymbol{x})$, i.e

$$\boldsymbol{ug}_i^h(\boldsymbol{x}_j) = (0, g(t_i)), \quad for \quad j = N_n + 1, ..., N$$

   But $\boldsymbol{ug}_i^h(\boldsymbol{x})$ can be written using the Lagrange functions $\phi_r(\boldsymbol{x}),\ \ r = 1, ..., N$ as,

$$\boldsymbol{ug}_i^h(\boldsymbol{x}) = (0, \sum_{r=N_n+1}^{N} g(t_i)\phi_r(\boldsymbol{x})) \tag{3.26}$$

   From (3.20) and (3.26) it follows that the approximation $\boldsymbol{u}_i^h + \boldsymbol{ug}_i^h$ to the solution of problem (3.1) with boundary conditions (3.2) and (3.3) can be written as

$$\boldsymbol{ug}_i^h(\boldsymbol{x}) + \boldsymbol{u}_i^h(\boldsymbol{x}) = \sum_{r=1}^{2N} \widetilde{d}_r^i \boldsymbol{\psi}_r(\boldsymbol{x}) \tag{3.27}$$

   where

$$\widetilde{\boldsymbol{d}}^{\,i} = (\widetilde{d}_1^i, ..., \widetilde{d}_{2N_n}^i, ..., \widetilde{d}_{2N}^i) = (d_1^i, d_2^i, ..., d_{2N_n}^i, 0, g(t_i), 0, g(t_i), ..., 0, g(t_i)).$$

4. COMPUTING DISPLACEMENTS WITH FREEFEM++

To solve numerically the wave propagation equations we use FreeFem++ [13], a free and open source software developed by mathematicians from Pierre et Marie Curie University of Paris. It runs on UNIX OS, Windows XP, Vista and 7, 8, 10 and on MacOS 10 Intel. This software computes the numerical solution using the variational formulation of the problem.
Procedure 1 contains a pseudocode with the main FreeFEM++ steps for computing the displacements, given the frequency f_0. The input of this procedure are the parameters describing the geometry $(L_x, L_y, \kappa, \theta)$ and the material (λ, μ, ρ) and also the final time t_f, the time step Δt and the pulse $g(t)$. The output of the

procedure are the vectors $\widetilde{\boldsymbol{d}}^{\,i}$ of coefficients in (3.27) of the approximated solution $\boldsymbol{ug}_i^h(\boldsymbol{x}) + \boldsymbol{u}_i^h(\boldsymbol{x})$ for $i = 1, ..., N$.
In order to describe the physical domain, it is necessary to parametrize the boundary curve of Ω, which is split in 4 parametric curves intersecting in their endpoints,

- $\mu_1(\alpha) = (X_1(\alpha), Y_1(\alpha))$, $\alpha \in [0, 1]$ is the circular arc corresponding to the bottom of the plate.
- $\mu_2(\alpha) = (X_2(\alpha), Y_2(\alpha))$, $\alpha \in [0, 1]$ is the straight line from the last point of μ_1 to the first point of μ_3.
- $\mu_3(\alpha) = (X_3(\alpha), Y_3(\alpha))$, $\alpha \in [0, 1]$ is the circular arc corresponding to the top of the plate.
- $\mu_4(\alpha) = (X_4(\alpha), Y_4(\alpha)) = \delta_2(\alpha)$, $\alpha \in [0, 1]$ is the straight line from the last point of μ_3 to the first point of μ_1.

The FreeFem++ code to generate the boundary curves $\mu_i(\alpha), i = 1, ..., 4$ is given in lines 1-4 of Procedure 1. Given a set of points on $\partial\Omega$, FreeFem++ uses the Delaunay-Voronoi algorithm to construct a triangulation τ^h of Ω, containing these points as vertices of τ^h. It is assumed that Ω is defined to the left of its oriented parameterized boundary. The keyword *buildmesh* is used in FreeFem++ to construct the triangulation τ^h, see line 7 of Procedure 1, where $n_x + 1$ is the number of vertices uniformly distributed on μ_1 and μ_3 and $n_y + 1$ is the number of vertices uniformly distributed on μ_2 and μ_4. Choosing $n_x = \lfloor n_y \frac{L_x}{L_y} \rfloor$, the triangles of τ^h are as close as possible to isosceles and consequently τ^h is a quasi-uniform and shape regular triangulation fitted to Ω [4]. In terms of n_y, the size of the corresponding triangular mesh τ^h is $h = \frac{\sqrt{2}\, L_y}{n_y}$.
The finite element space $\mathcal{V}_0^h$ defined in (3.15), is built in line 9 of Procedure 1, where *P2* denotes the quadratic Lagrange finite element. For this type of elements, the total number of degrees of freedom *dof* can be written in terms of n_y and it is equal to $400n_y^2 + 204n_y + 2$. Line 12 defines the variational formulation of the problem with the keyword *varf* and uses *int2d* to compute the double integral over τ^h. The keyword *on* imposes the Dirichlet boundary condition.
The Cholesky factorization $\mathbf{A}_{chol}$ of the matrix $\mathbf{A}$ given in (3.23) is computed in line 14 with the keyword *matrix*. To impose Dirichlet condition on μ_4 keyword *tgv* is used. Lines 15-20 contain a loop for computing the right hand sides $\boldsymbol{b}^i$ of systems (3.22) and the corresponding solutions $\boldsymbol{d}^i$ computed using Cholesky factorization of $\mathbf{A}$.
Based on the Procedure 1 we develop a FreeFem++ code to compute the displacement field after emitting a pulse of frequency f_0, for a sequence of times t_i in $[0, t_f]$. In all experiments of this work, the mesh size h and the time step Δt are chosen in such away that the *CFL condition* (after R. Courant, K. Friedrich and H. Lewy) $\Delta t < \frac{h}{C(f_0)}$ holds, as recommended in the literature [2, 8, 25].
In Figure 3 we show the vertical deformation field of a curved steel plate of length $L_x = 5 \cdot 10^{-2} m$, thickness $L_y = 1 \cdot 10^{-3} m$ and curvature $\kappa = 0.5\ m^{-1}$. The frequency of the pulse is $f_0 = 0.5\ MHz$. Colors in this figure correspond to the intensity of the vertical deformation field (the norm of the vertical displacement).

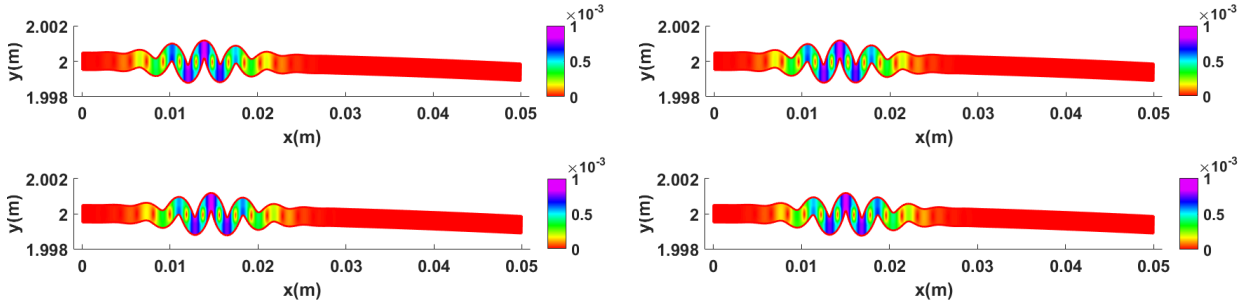

Figure 3: Graphics for $t = 9.8 \cdot 10^{-5}\ s$, $t = 1 \cdot 10^{-4}\ s$ (top row), $t = 1.02 \cdot 10^{-4}\ s$ and $t = 1.04 \cdot 10^{-4}\ s$ (bottom row) of the vertical deformation field of a curved steel plate with curvature $\kappa = 0.5\ m^{-1}$, after emitting a pulse on δ_2. Colors correspond to the intensity of the vertical deformation field.

Section 5.2. contains details about the computational cost of the numerical solution of the wave propagation equations. This is the most expensive step of *PVM-FEM* method to compute dispersion curves.

Procedure 1 Computing Displacements

Input: Geometry $(L_x, L_y, \kappa, \theta)$, material constants (λ, μ, ρ), frequency f_0, final time t_f, time step Δt, pulse $g(t)$.

for $i = 1$ to 4 **do**
  // Parametrize boundary curve $\mu_i(\alpha) = (X_i(\alpha), Y_i(\alpha))$
  $border\ \ \mu_i\,(\alpha = 0, 1)\,\{x = X_i(\alpha); y = Y_i(\alpha);\ label = i;\}$
end for
Select n_y and set $n_x = \lfloor n_y \frac{L_x}{L_y} \rfloor$
// Build a triangulation τ^h *on* Ω
$mesh\ \ \tau^h = buildmesh\ \ (\mu_1(n_x + 1) + \mu_2(n_y + 1) + \mu_3(n_x + 1) + \mu_4(n_y + 1))$
// Define the finite element space $\mathcal{V}_0^h$
$fespace\ \ \mathcal{V}_0^h(\tau^h, [P2, P2])$
Compute $\boldsymbol{u}_1^h(\boldsymbol{x})$ using finite differences and $\boldsymbol{u}_0^h(\boldsymbol{x}) = \boldsymbol{u}_{-1}^h(\boldsymbol{x}) = \mathbf{0}$
// Define variational formulation
$varf\ \ a(\mathbf{u}, \mathbf{v}) = int2d\left(\tau^h\right)\left(2\rho(\mathbf{u}\cdot\mathbf{v}) + \left(\Delta t^2\right)\left(\nabla\cdot\boldsymbol{\sigma}(\boldsymbol{u})\cdot\boldsymbol{v}\right)\right) + on(4, u_x = 0, u_y = g)$
// Build Cholesky factorization $\mathbf{A}_{chol}$ *of matrix* $\mathbf{A}$
$matrix\ \mathbf{A}_{chol} = a(\mathcal{V}_0^h, \mathcal{V}_0^h, solver = Cholesky, factorize = 1, tgv = 1)$
for $i = 2$ to N **do**
  // Compute the right hand side for $t = t_i = i \cdot \Delta t$
  $\boldsymbol{b}^i = \boldsymbol{M} * (5\boldsymbol{d}^{i-1} - 4\boldsymbol{d}^{i-2} + \boldsymbol{d}^{i-3})$
  // Solve the linear system using Cholesky factorization of $\boldsymbol{A}$
  $\boldsymbol{d}^i = \boldsymbol{A}_{chol}\texttt{\^{}-1} * \boldsymbol{b}^i$
end for

Output: Vector $\widetilde{\boldsymbol{d}}^{\,i}$, $i = 1, ..., N$ of coefficients in (3.27) of the approximated solution $\boldsymbol{ug}_i^h(\boldsymbol{x}) + \boldsymbol{u}_i^h(\boldsymbol{x})$.

5. PHASE VELOCITY DISPERSION CURVE

In dispersive media the phase velocity C of the wave depends on the frequency f_0. This dependence is described by the phase velocity dispersion curves. In the case of thin plates with constant thickness L_y, the phase velocity dispersion curve is the parametric curve [23],

$$(f_0 \cdot L_y/2\,,\, C(f_0)) \tag{5.1}$$

In this section we explain how to compute the phase velocity $C(f_0)$ from the displacement fields obtained solving the wave equations for a given frequency f_0.

5.1. *FEM-PVM* for isotropic curved plates with constant thickness

In this work the *FEM-PVM* approach is used to compute $C(f_0)$ for a set of frequencies f_0. The general idea of this method is the following. For each value of f_0, the wave propagation equations for a pulse depending on f_0 are solved with FEM. From the FEM solution we obtain the displacements $u_y(t, \mathbf{p}_i)$ of the plate in the vertical direction at selected points $\mathbf{p}_i$ (receivers) on the top of the plate, as functions on time. The vertical displacement functions are used to compute the arrival time at receivers of a fixed phase point of the pulse. Finally, with these arrival times and the arc length distances between the receivers, the phase velocity $C(f_0)$ corresponding to the given frequency f_0 is computed.
In order to illustrate how *FEM-PVM* works we compute the phase velocity $C(f_0)$ for $f_0 = 0.5\,MHz$ in a typical steel plate with dimension $L_x = 5.0 \cdot 10^{-2}\ m$, constant thickness $L_y = 1.0 \cdot 10^{-3}\ m$ and curvature $\kappa = 0.5\ m^{-1}$. Since the material is isotropic, the elastic constants involved in the formulation of the problem are given by $C_{66} = \mu$, $C_{12} = \lambda$ and $C_{11} = C_{22} = \lambda + 2\mu$, where λ and μ are the Lamé constants. The

Lamé constants, and the density ρ of the steel are given in table 1. On the top of the plate 6 receivers with coordinates $\mathbf{p}_i = (x_i, y_i) = \left(R_2 \sin\left((i+4)\,\frac{L_y}{R_2}\right), R_2 \cos\left((i+4)\,\frac{L_y}{R_2}\right)\right)\ i = 1, ..., 6$ are fixed, where R_2 is the external circle radius, see Figure 4.

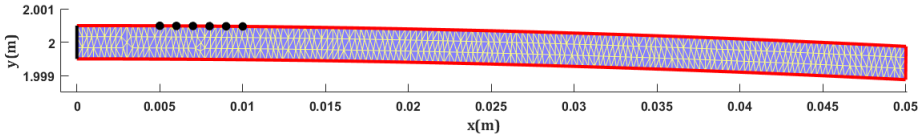

Figure 4: Thin curved plate guidewave with selected receivers $\boldsymbol{p}_i,\ i = 1, ..., 6$ on the top.

Figure 5 left shows, for each fixed receiver $\mathbf{p}_i,\ i = 1, ..., 6$, the function interpolating the sequence of vertical displacements $u_y(t_j, \mathbf{p}_i)$ computed with FEM, for the values of $t_j = j\,\Delta t,\ j \geq 0$. The arrival time $\widetilde{t}_i$ of the pulse at the point $\mathbf{p}_i,\ i = 1, ..., 6$ is computed as the value of t for a selected maximum (represented in Figure 5 as a red bullet) of the function $u_y(t, \mathbf{p}_i)$. It holds that for a given value of f_0, the points $(\widetilde{t}_i, l_i),\ i = 1, ..., 6$ are approximately on a line, where $l_i = 2R_2 \arctan\left(\frac{\|\mathbf{p}_{i+1} - \mathbf{p}_i\|}{2R_2}\right)$ is the arc length between $\mathbf{p}_i$ and $\mathbf{p}_{i+1}$. The slope of this line is the phase velocity $C(f_0)$ corresponding to the frequency f_0. Figure 5 right shows the points $(\widetilde{t}_i, l_i),\ i = 1, ..., 6$ and the fitting line.

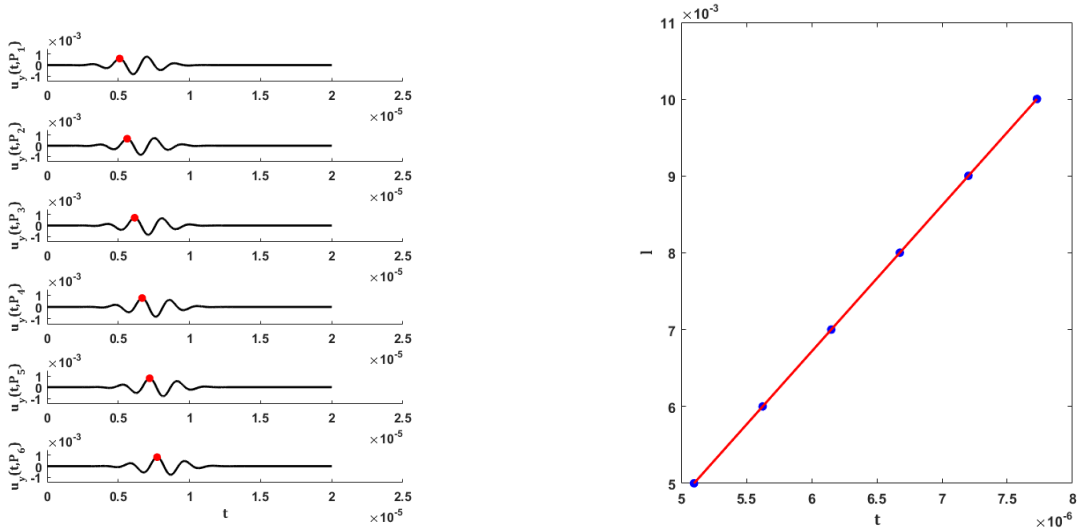

Figure 5: Left: Graphic of the displacement in the vertical direction $u_y(t, \boldsymbol{p}_i)$ of the selected receivers $\boldsymbol{p}_i = (x_i, y_i),\ i = 1, ..., 6$, for $f_0 = 0.5\,MHz$. Red bullets: point on $u_y(t, \boldsymbol{p}_i)$ corresponding to the arrival time $\widetilde{t}_i$ of the pulse at the point $\boldsymbol{p}_i,\ i = 1, ..., 6$. Right: Plot of l_i versus arrival times $\widetilde{t}_i$, for $i = 1, ..., 6$ and the fitting line.

5.2. Discussion of numerical results

In this section we summarize the results of an extensive numerical experimentation for computing the phase velocity dispersion curves of several plates. All considered plates have the same dimension $L_x = 5.0 \cdot 10^{-2}\ m$ and constant thickness $L_y = 1.0 \cdot 10^{-3}\ m$, but different curvature values (in m^{-1}):

$$\kappa = 0.01,\ 0.5,\ 1.0,\ 10.0,\ 25.0,\ 50.0. \tag{5.2}$$

We consider curved plates of two materials: steel and aluminium. The Lamé constants, and the density ρ for these material are given in table 1.

material	$\mu\ (N/m^2)$	$\lambda\ (N/m^2)$	$\rho\ (kg/m)$
steel	$7.692 \cdot 10^{10}$	$1.154 \cdot 10^{11}$	7 850
aluminium	$2.624 \cdot 10^{10}$	$5.279 \cdot 10^{11}$	2 700

Table 1: Parameters of curved plate material.

The wave propagation equations are solved with *quadratic* FEM, for pulses $g(t)$ with 10 different frequencies (in MHz):

$$f_0 = 0.1,\ 0.2,\ 0.3,\ 0.4,\ 0.5,\ 0.7,\ 0.9,\ 1.1,\ 1.3,\ 1.5 \tag{5.3}$$

In total we compute 10 points (one for each f_0) on the phase velocity dispersion curve of 12 plates. It means that wave equations are solved 120 times. All calculations were done in a PC with $i7-8565U$ processor and 8 Gb of RAM.

The computation of the displacement field in the interval $[0, t_f]$ is the most expensive step of *FEM-PVM*, for obtaining dispersion curves. To illustrate the computational cost in CPU time of this step, we show in table 2 the results for a typical experiment corresponding to an aluminium plate with curvature $\kappa = 0.5\ m^{-1}$. It is well known that phase velocity increases with the frequency f_0, hence the arrival time to the last receiver decreases with f_0, and in order to apply *FEM-PVM* it is enough to solve the wave equations for an interval $[0, t_f]$, with t_f decreasing with f_0, see column 2 of table 2. The time step Δt reported in the third column was always $\Delta t = 10^{-8}$ since for this values it holds $\Delta t \leq \frac{1}{20\, f_0}$ for all considered frequencies. Wave equations are solved with *quadratic* FEM using a triangular mesh, with size h decreasing for increasing f_0. The mesh size h and the number of triangles of the mesh are shown in columns 4 and 5 respectively. The size of the matrix $\mathbf{A}$ of the linear systems (3.22) is given in column 6. In column 7 we report the CPU time (in seconds) needed to compute the Cholesky factorization of two matrices: the matrix of the variational problem for $t = t_1$ and the matrix $\mathbf{A}$. The last column shows for each frequency f_0, the total CPU time to compute the displacements in the interval $[0, t_f]$. Adding up the times reported in the last column of Table 2 we obtain that the total time for computing the displacements for the 10 values of considered frequencies is 7.68 minutes.

$f_0\,(MHz)$	$t_f\,(s)$	$\Delta t\,(s)$	$h\,(m)$	# of triangles	size of $\mathbf{A}$	Cholesky CPU time (s)	Total CPU time (s)
0.1	$5.0 \cdot 10^{-5}$	$1 \cdot 10^{-8}$	$2.65 \cdot 10^{-4}$	3 854	16 638	0.115	25.375
0.2	$3.0 \cdot 10^{-5}$	$1 \cdot 10^{-8}$	$2.65 \cdot 10^{-4}$	3 854	16 638	0.200	15.235
0.3	$2.5 \cdot 10^{-5}$	$1 \cdot 10^{-8}$	$2.65 \cdot 10^{-4}$	3 854	16 638	0.115	12.018
0.4	$2.5 \cdot 10^{-5}$	$1 \cdot 10^{-8}$	$2.65 \cdot 10^{-4}$	3 854	16 638	0.200	12.277
0.5	$2.0 \cdot 10^{-5}$	$1 \cdot 10^{-8}$	$2.65 \cdot 10^{-4}$	3 854	16 638	0.115	10.018
0.7	$2.0 \cdot 10^{-5}$	$1 \cdot 10^{-8}$	$1.05 \cdot 10^{-4}$	23 064	95 314	1.511	87.824
0.9	$2.0 \cdot 10^{-5}$	$1 \cdot 10^{-8}$	$1.05 \cdot 10^{-4}$	23 064	95 314	1.449	87.569
1.1	$1.5 \cdot 10^{-5}$	$1 \cdot 10^{-8}$	$1.05 \cdot 10^{-4}$	23 064	95 314	1.970	69.308
1.3	$1.5 \cdot 10^{-5}$	$1 \cdot 10^{-8}$	$1.05 \cdot 10^{-4}$	23 064	95 314	1.653	69.734
1.5	$1.5 \cdot 10^{-5}$	$1 \cdot 10^{-8}$	$1.05 \cdot 10^{-4}$	23 064	95 314	1.659	71.335

Table 2: Numerical results for a curved aluminum plate with curvature $\kappa = 0.5\ m^{-1}$

The results for the rest of 11 curved plates included in the experiments are omitted since they are similar to the reported in table 2. It is worth to mention that the maximum CPU time to solve the wave equations for a frequency f_0 was 89.124 s. It was obtained for the steel plate with curvature $\kappa = 0.01\ m^{-1}$ for $f_0 = 0.7\ MHz$.

Once we have obtained the displacements for each frequency f_0 in (5.3), the corresponding phase velocity $C(f_0)$ is computed using the methodology explained in the previous section. Finally, the points $(f_0 \frac{L_y}{2}, C(f_0))$

on the dispersion curve are fitted with a *rational quadratic curve* that provides a good fit, both in regions with high slope (small frequency), as well as in regions with asymptotic behavior (high frequency).
To exemplify the results we show in Figure 6 the phase velocity dispersion curves computed with *FEM-PVM* corresponding to three steel plates with curvatures $\kappa = 0.01\ m^{-1}$ (black), $\kappa = 25\ m^{-1}$ (red) and $\kappa = 50\ m^{-1}$ (blue). Moreover, the dispersion curves for steel and aluminium plates with the same curvatures and thickness are compared in Figure 7.

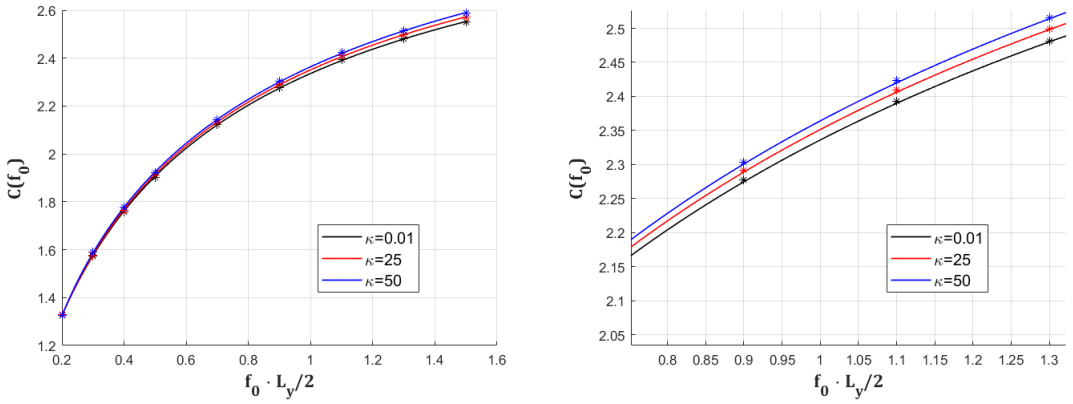

Figure 6: Left: dispersion curves of a curved steel plate for $\kappa = 0.01\ m^{-1}$ (black), $\kappa = 25\ m^{-1}$ (red) and $\kappa = 50\ m^{-1}$ (blue). Right: zoom. The units are: f_0 in MHz, L_y in mm and $C(f_0)$ in Km/s.

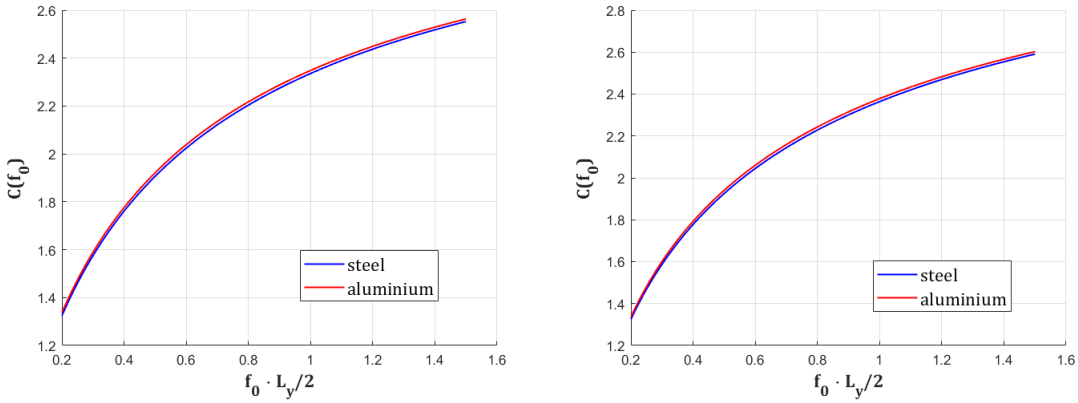

Figure 7: Dispersion curves of curved plate guidewaves with thickness $L_y = 1.0 \cdot 10^{-3} m$ and frequencies f_0 in the interval $[0.2\ MHz, 1.5\ MHz]$. Left: $\kappa = 0.1\ m^{-1}$, right: $\kappa = 50\ m^{-1}$.

Summarizing, our experiments computing with *FEM-PVM* the phase velocity dispersion curves for steel and aluminium plates with the same dimensions suggest that:

- The phase velocity curves of plates of both materials with same curvature have similar behavior. For a given frequency f_0 the value of $C(f_0)$ of the aluminium plate is greater than the value of $C(f_0)$ of the steel plate.

- The phase velocities of curved plates converge to the phase velocities of the flat plate with the same constant thickness, when the curvature tends to zero.

- For the same thickness, small differences in the curvature correspond to very close dispersion curves.
- Plates with higher curvatures have higher phase velocities.
- The difference of phase velocities corresponding to plates with distinct curvatures increases with the frequency. For small frequencies this difference is very small and may be neglected. On the other hand, for frequencies higher than $1\,MHz$ the phase velocities differences are more considerable. Hence, frequencies higher than $1\,MHz$ are good candidates to detect defects.

6. CONCLUSIONS

Dispersion curves are very useful to evaluate defects such as corrosion or delaminations in thin plates. The results of this work show that Phase Velocity Method can be successfully used in combination with Finite Element Method to compute phase velocity dispersion curves of thin annular isotropic plates.
We have implemented *FEM-PVM* approach with the open source software FreeFem++ using quadratic Lagrange triangular finite element and modest computational resources. The code, available at GitHub in [5], was used to study the performance of *FEM-PVM* through an extensive numerical experimentation, with plates of two materials and different curvatures. For constant thickness curved plate guidewaves, for which analytical dispersion curves are unknown, the numerical results show that *FEM-PVM* provide information on the behavior of the phase velocity dispersion curves with respect to variations of the curvature. In particular, we have observed that plates of the same thickness and material but different curvatures have similar phase velocity dispersion curves, and for the same frequency, the higher phase velocity corresponds to the plate with higher curvature. Moreover, the difference of phase velocities corresponding to plates with distinct curvatures increases with the frequency. Thus, frequencies higher than $1\,MHz$ are recommended to detect defects.
More simulations should be done in the future to compare the numerical results with laboratory experiments. *FEM-PVM* could be also used in other problems, where theoretical dispersion curves are unknown, such as in the case of more complicated geometries or nonelastic and anisotropic materials. Due to the importance of the dispersion curves for industrial applications, this subject will be treated in a future research.

RECEIVED: MARCH, 2022.
REVISED: JANUARY, 2023.

REFERENCES

[1] J. D. ACHENBACH, (1973): **Wave Propagation in Elastic Solids**, North-Holland, New York.

[2] K.J. BATHE (1996): **Finite element procedures**, Prentice Hall.

[3] A. S. BIRKS, R. E. GREEN, P. MCINTIRE, (1991): **Nondestructive testing handbook, Vol. 7.** Ultrasonic Testing, American Society for Nondestructive Testing Inc, Second Edition. ISBN: 9780931403040

[4] P.G. CIARLET (1979): **The finite element method for elliptic problems, Studies in mathematics and its applications**, North-Holland Pub. Co..

[5] M. CRUZ, A. MANSUR, E. MORENO, V. HERNÁNDEZ AND J. ESTRADA, Wave Propagation Code with FreeFEM, https://github.com/MathICIMAF/Wave-Propagation-Code-with-FreeFEM.

[6] M. CRUZ, V. HERNÁNDEZ, J. ESTRADA, E. MORENO AND A. MANSUR (2021): Numerical Solution of the Wave Propagation Problem in a Plate**Journal of Theoretical and Computational Acoustics** 2150014. DOI: 10.1142/S2591728521500146.

[7] M. CRUZ, E. MORENO, V. HERNÁNDEZ, J. ESTRADA, A. MANSUR (2021): Phase velocity method for computing dispersion curves in thin plates, **International Ultrasonic Testing Conference 2021** (UT-Online 2021), NDT.net Issue: 2021–11, 2021.

[8] M.B. DROZDZ, (2008): **Efficient Finite Element modelling of ultrasound waves in elastic media,** Ph.D. Thesis, Imperial College of Science Technology and Medicine, University of London, UK.

[9] M. E. C. EL-KETTANI, F. LUPPÉ AND A. GUILLET (2004): Guided waves in a plate with linearly varying thickness: experimental and numerical results, **Ultrasonics**, 42, 807-812.

[10] J. FONG AND M. J. S. LOWE (2004): Curvature effect on the properties of guided waves in plates, **Review of Quantitative Nondestructive Evaluation**, 23, ed. by D. O. Thompson and D. E. Chimenti, American Institute of Physics.

[11] J. M. GALÁN AND R. ABASCAL (2002): Numerical simulation of Lamb wave scattering in semi-infinite plates, **Int. J. Numer. Methods Eng.**, 53, 1145-1173.

[12] T. HAYASHI, W. J. SONG AND J. L. ROSE (2003): Guided wave dispersion curves for a bar with an arbitrary cross-section, a rod and rail example, **Ultrasonics**, 41, 175–183, .

[13] F. HECHT (2012): New development in FreeFem++, **J. Numer. Math.** 20, 251–265.

[14] M. LARSON, F. BENGSON (2013): **The Finite Element Method: Theory, Implementation and Applications**, Springer Verlag.

[15] M. J. S. LOWE, D. N. ALLEYNE AND P. CAWLEY (1998): Defect detection in pipes using guided waves, **Ultrasonics**, 36, 147–154.

[16] G. MARTINCEK (1974): La diagnose de l'élasticité dynamique et de la rigidité des structures routiéres a l'aide de la méthode de vitesses de phase des ondes de contrainte', In: **New Developments in Non-Destructive Testing of Non-Metallic Materials.** RILEM, Constanta, 35-42.

[17] G. MARTINCEK AND T. KADLECIK (1982): The Use of Wave Propagation Methods in Evaluation of Road Pavements Stiffnes, **Proc. Int. Symp. on Bearing Capacity of Roads and Airfields**, 1, 119–127, Trondheim.

[18] E. MORENO AND P. ACEVEDO (1998): Thickness measurement in composite materials using Lamb waves, **Ultrasonics**, 35, 581–586.

[19] E. MORENO, P. ACEVEDO AND M. CASTILLO (2003): Pulse propagation in plate elements, **European Journal of Mechanics A, Solids**, 22, 283–294.

[20] E. MORENO, N. GALARZA, B. RUBIO AND J. A. OTERO (2015): Phase velocity method for guided wave measurements in composite plates, in **UIA Symposium 2014, Physics Procedia**, 63, 54–60.

[21] A. H. ORTA, M. KERSEMANS, K. VAN DEN ABEELE (2022): A comparative study for calculating dispersion curves in viscoelastic multi-layered plates, **Composite Structures**, 294, 115779. DOI: 10.1016/j.compstruct.2022.115779.

[22] M. V. M. PREDOI, M. E. C. EL-KETTANI, Z. HAMITOUCHE AND C. C. PETRE (2008): Guided waves in plates with linear variation of thickness, **The Journal of the Acoustical Society of America**. DOI: 10.1121/1.2935622.

[23] J. L. ROSE (1999): **Ultrasonic Waves in Solid Media**, Cambridge University Press, Cambridge.

[24] R. WEBER, S. M. H. HOSSEINI AND U. GABBERT (2012): Numerical Simulation of the Guided Lamb Wave Propagation in Particle Reinforced Composites, **Composite Structures**, 94, 3064–3071, .

[25] C. WILLBERG, S. DUCZEK, J. M. V. PEREZ, D. SCHMICKER AND U. GABBERT (2012): Comparison of different higher order finite element schemes for the simulation of Lamb waves, **Comput. Methods Appl. Mech. Eng.**, 518, 95–105.